Biochemistry and Biophysics Reports 10 (2017) 62–69

Contents lists available at ScienceDirect

Biochemistry and Biophysics Reports

journal homepage: www.elsevier.com/locate/bbrep

Synthesis and characterization of pHLIP® coated gold nanoparticles

Jennifer L. Daniels, Troy M. Crawford, Oleg A. Andreev, Yana K. Reshetnyak*

Physics Department, University of Rhode Island, 2 Lippitt Rd., Kingston, RI 02881, USA

ARTICLE INFO

Keywords:
Spherical gold nanoparticles
Spiked gold nanoparticles
Disk-like bicelles
Hyperthermia
Tumor targeting
Acidity

ABSTRACT

Novel approaches in synthesis of spherical and multispiked gold nanoparticles coated with polyethylene glycol (PEG) and pH Low Insertion Peptide (pHLIP®) were introduced. The presence of a tumor-targeting pHLIP® peptide in the nanoparticle coating enhances the stability of particles in solution and promotes a pH-dependent cellular uptake. The spherical particles were prepared with sodium citrate as a gold reducing agent to form particles of 7.0 ± 2.5 nm in mean metallic core diameter and ~43 nm in mean hydrodynamic diameter. The particles that were injected into tumors in mice (21 μg of gold) were homogeneously distributed within a tumor mass with no staining of the muscle tissue adjacent to the tumor. Up to 30% of the injected gold dose remained within the tumor one hour post-injection. The multispiked gold nanoparticles with a mean metallic core diameter of 146.0 ± 50.4 nm and a mean hydrodynamic size of ~161 nm were prepared using ascorbic acid as a reducing agent and disk-like bicelles as a template. Only the presence of a soft template, like bicelles, ensured the appearance of spiked nanoparticles with resonance in the near infrared region. The irradiation of spiked gold nanoparticles by an 805 nm laser led to the time- and concentration-dependent increase of temperature. Both pHLIP® and PEG coated gold spherical and multispiked nanoparticles might find application in radiation and thermal therapies of tumors.

1. Introduction

Gold nanoparticles (ranging in size from 1 to 200 nm) might find various applications in medicine including the enhancement of x-ray radiation damage to tumor tissues [1–4] and the induction of localized heating in photothermal therapy [5–7]. The latter is achieved when gold nanoparticles are exposed to light and impart heat energy to their local environment due to the temporary existence and decay of localized surface plasmon polaritons. In addition of use of gold nanoparticles, also supermagnetic nanoparticles are developed for magnetic resonance imaging and hyperthermia to induce cancer cells death or promote drug release [8–13]. In all cases of nanoparticle use, not only should the particles be stable, but they should preferentially target diseased tissue, such as a cancerous tumor.

Many contemporary therapeutic and imaging approaches to cancer treatment rely on tumor-targeting biomarkers such as antibody technologies or vitamin binding [14–18]. Although there are significant successes, the inter- and intra-heterogeneity of tumors, their complexity, and their ability to adapt to new conditions often create parts of a tumor that may not express enough of the biomarker to be targeted. This results in the regrowth of resistant tumors and poor therapeutic outcomes, where the average improvements in survival are measured in months. At the same time, there is an emerging body of evidence indicating that the acidity of the tumor tissue plays a key role in determining cancer cell invasiveness and resistance to therapies. Tumors exhibit marked heterogeneity due to genetic alterations, which lead to the modification of biochemical pathways. The modifications that result from metabolic alterations, lead to a surge in extracellular acidity. Tumor cells adapt to this acid-induced toxic environment by stimulating proteins that regulate intracellular homeostasis [19,20].

Among pH-targeting agents, the family of pH Low Insertion Peptides (pHLIP®) find a broad range of applications in biomedical sciences. pHLIP® peptides insert across cellular membranes in a pH-dependent manner, with one terminus exposed to the extracellular space and the other terminus to the cytoplasm [21–24]. The molecular mechanism of a pHLIP® peptide's action is based on the protonation of Asp/Glu residues, which enhances the peptide's hydrophobicity and promotes membrane-associated folding with the insertion of a transmembrane helix [25,26]. It was shown that pHLIP® peptides are excellent at targeting acidic tumors, which allows for the specific delivery of imaging and therapeutic agents to cancer cells within tumors [22,27–29]. The number and variety of pHLIP® based nanomedicines is growing. For example, the coating of lipid-based, polymeric, and metallic nanoparticles with pHLIP® peptides enhances the targeting of acidic tumors and the number of particles internalization within cancer cells [30–36].

* Corresponding author.
E-mail address: reshetnyak@uri.edu (Y.K. Reshetnyak).

http://dx.doi.org/10.1016/j.bbrep.2017.02.008
Received 16 December 2016; Received in revised form 19 February 2017; Accepted 26 February 2017
Available online 28 February 2017

We have shown specific tumor accumulation of gold nanoclusters of 1.4 nm in diameter conjugated to the pHLIP® peptide [37], and an enhancement of radiation effect observed for cancer cells treated with pHLIP® gold nanoclusters [38]. As well, novel photo-induced pHLIP® coated hollow gold nanospheres containing chlorin e6 were introduced recently [33,34]. The nanospheres experience hyperthermia within 5 min of laser exposure, which leads to the release of photosensitizers due to the reduction of electrostatic interaction. While the obtained results are very interesting and promising, there are aspects which require improvement and justify further work: i) the coating of gold nanoclusters conjugated with pHLIP® peptide should be improved to avoid particles aggregation; and ii) a greater amount of gold might be needed in tumors to observe a significant radiation enhancement effect. Therefore, here we introduce novel approaches for synthesis of pHLIP® and PEG coated spherical and spiked gold nanoparticles for the enhancement of radiation damage and near infrared (NIR) thermal therapy.

2. Materials and methods

2.1. Materials for synthesis of pHLIP® and PEG coated gold nanoparticles

Gold III chloride, 5% solution, was purchased from Salt Lake Metals (Salt Lake City, UT). Sodium citrate tribasic, L-ascorbic acid, and urea dehydrate were purchased from Sigma-Aldrich Co. (St. Louis, MO). The wild type (WT) pHLIP® peptide:

ACEQNPIYWARYADWLFTTPLLLLDLALLVDADET

was synthesized and purified by C.S. Bio Co. (Menlo Park, CA), and the concentration of the peptide was determined by absorbance at 280 nm ($\varepsilon = 13{,}940\ M^{-1}\ cm^{-1}$). The m-polyethylene glycol–SH (mPEG-SH), about 5 kDa in mass, was purchased from Creative PEGworks (Chapel Hill, NC). The lipids, 1,2-dihexanoyl-*sn*-glycero-3-phosphocholine, D6PC; 1,2-diheptanoyl-*sn*-glycero-3-phosphocholine, D7PC/DHPC and 1,2-dimyristoyl-*sn*-glycero-3-phosphocholine, DMPC were purchased from Avanti Polar Lipids, Inc (Alabaster, AL). Tris-(2-carboxyethyl)phosphine hydrochloride (TCEP) was purchased from Thermo Fisher Scientific (Waltham, MA). The procedures for synthesis of the spherical and multispiked pHLIP® and PEG coated gold nanoparticle are described in the Results section.

2.2. Bicelle preparation

Bicelles were prepared by thin-film method: a chloroform solution of DMPC and D7PC (DHPC) lipids were dried using a rotary evaporator producing an even thin film, followed by the additional overnight evaporation under a high vacuum to remove traces of organic solvents. The lipid layer was re-suspended in 10 mM phosphate buffer pH 6.5 and underwent ten freeze-thaw-vortex cycles using liquid nitrogen and a warm bath (40 °C).

2.3. Purification of gold nanoparticles

To remove large particles (in the case of spherical gold nanoparticles) and excess reducing agents, the final solution of particles underwent two forms of filtration. Large particles were removed using centrifugation (5 min at 10,000 relative centrifugal force, RCF). Excess reducing agents were removed by size-exclusion chromatography using sephadex G25 fast spin columns. 500 µL of particles was added to 5 mL of sephadex G25 gel filtration beads (Sigma-Aldrich Co.) (the beads were hydrated in the desired buffer) and centrifuged for 0.5 min increments at roughly 36 RCF. The final nanoparticle solutions were passed through a 0.2 µm sterile Acrodisk® syringe filter with HT Tuffryn® membrane (Pall Life Sciences) for sterilization when experiments on cultured cells and mice were carried out, as well as for stability studies and heating experiments.

2.4. UV–visible absorption spectroscopy

The absorbance of gold nanoparticles was recorded on a Genesys 10S UV–Vis Spectrophotometer to establish the wavelength range of resonance.

2.5. Measurements of particles size

The size of bicelles and gold nanoparticles in solution was measured by dynamic light scattering (DLS) using a Zetasizer Nano ZS (Malvern) instrument and a nanoparticle tracking system, Nanosight (NS300, Malvern), respectively. Transmission electron microscopy (TEM) (JEOL 2100) with an accelerating voltage of 200 kV at magnifications in the range of 10,000× to 150,000× was used to image gold nanoparticles to establish the shape, size, and homogeneity of the particles. Samples were prepared for TEM by drying 5 µL of the nanoparticle solution on a carbon type-B, 300 mesh, copper grid (Ted Pella, Inc). Size histograms were averaged and fitted with a Gaussian function.

2.6. ICP-MS analysis

The investigated samples (cells, tumor tissue, or nanoparticles in solution) were dissolved in a concentrated solution of aqua regia (1:3 volume ratio of nitric acid and hydrochloric acid) and sonicated. The final solutions were diluted to 2% (wt/vol) nitric acid with distilled water and centrifuged to remove organic tissue. The gold content was quantified using inductively coupled plasma mass spectrometry (ICP-MS) (Thermo scientific X7 series and Thermo X-Series 2 quadrupole) by using calibration standards IMS 103 (UltraScientific).

2.7. Heating

In a poly(methyl methacrylate) (PMMA) cuvette (with a 4.5 mm window width and 12.5 mm depth), 300 µL of solution was illuminated by an 805 nm temperature controlled laser diode with 500 mW output (TCLDM9, Thorlabs). The solution temperature was measured every minute with an immobilized FLIR E6 thermal imager (FLIR Systems, Inc.) from above to avoid obstruction by the cuvette walls. A sample of phosphate-buffered saline (PBS), pH 7.4, was illuminated and used as a baseline.

2.8. Cancer cells

JC murine mammary-gland adenocarcinoma cells were obtained from the American Type Culture Collection (ATCC). The cells were cultured in Roswell Park Memorial Institute (RPMI) medium supplemented with 10% fetal bovine serum (FBS) and 10 µg/mL ciprofloxacin in a humidified atmosphere of 5% CO_2 and 95% air at 37 °C.

2.9. Cytotoxicity assay

JC cancer cells were seated in a 96-well plate (3000–3500 cells per well in 100 µL RPMI medium) and incubated overnight. The next day, 100 µL of gold nanoparticles in PBS pH 7.4 supplemented with 10 mM D-glucose were added to the cells at two concentrations and incubated for 48 h. Final gold concentrations after addition to cells were 0.025 g/L and 0.013 g/L (spherical particles) 0.010 g/L and 0.005 g/L (multi-spiked particles). Cell viability was assessed by a colorimetric reagent (CellTiter 96 AQ_{ueous} One Solution Assay, Promega), which was added to cells for one hour followed by the measurement of absorbance at 490 nm by an iMark Microplate Absorbance Reader (Bio-Rad Laboratories, Inc.). The absorbance readings were corrected for the absorbance of gold nanoparticles at 490 nm. All samples were prepared in triplicate.

2.10. Cellular uptake of gold nanoparticles

Various amounts of JC cancer cells (from 100,000 to 1 million cells in different experiments) were treated in suspension with purified spherical gold nanoparticles (0.83% citrate and 10% pHLIP-90% PEG) (typically the final concentration of gold with cells was 0.06 g/L) for three hours at 37 °C in serum-free Leibovitz's L-15 medium of pH 6.0 or pH 7.4 (final treatment volume was 500 μL). In another experiment, JC cells were pre-treated with gold nanoparticles in serum-free L-15 medium at pH 7.4 for 20 min, and then media (with different pHs) were added to set a total volume of 500 μL and a final solution pH of 7.4 or 6.0–6.2. After treatment, samples were pelleted (5 min at 600 RCF) and washed with PBS, pH 7.4, three times. The amount of gold in each pellet was then quantified using ICP-MS. The amount of gold not taken up by cells was quantified in the supernatant by absorbance measurements. Control samples of gold nanoparticles without cells and cells without particles were investigated at both high and low pH as well. All samples were prepared in triplicate.

2.11. Uptake and distribution of gold in tumors

All animal studies were conducted according to the animal protocol AN07-01-015 approved by the Institutional Animal Care and Use Committee at the University of Rhode Island, in compliance with the principles and procedures outlined in the National Institutes of Health Guide for the Care and Use of Animals. Female Balb/C mice ranging in age from 4 to 6 weeks and weighing from 18 to 22 g were obtained from Envigo RMS, Inc; 16 mice were used in the study. Tumors were established in the right flank by subcutaneous injection of JC cancer cells (10^6 cells in 100 μL). After about two weeks, 50 μL of 0.11 g/L of purified spherical gold nanoparticles (0.83% citrate and 10% pHLIP-90% PEG) (5.5 μg of gold), or 0.42 g/L gold particles (21 μg of gold) in PBS, pH 7.4, supplemented with 10 mM D-glucose were injected intratumorally. An hour after injection, mice were euthanized and the tumors were immediately collected for histological and gold-quantification analysis. The amount of gold in each tumor was quantified using ICP-MS. A non-injected mouse with a similar-sized tumor was used as a negative control. The distribution of gold within the tumor was assessed by white light imaging of the tumor center.

2.12. Histological staining and imaging of tumor sections

Immediately after tumors were collected from the mice, they were frozen in tissue-tek OCT compound using liquid nitrogen and stored at −80 °C until sectioned at a thickness of 20 μm using a cryostat at −25 °C (Vibratome UltraPro5000, GMI). Tumor sections were then fixed in a 4% paraformaldehyde solution (Sigma-Aldrich Co.), washed three times with deionized water, permeated with 0.3% Triton X-100 (Sigma-Aldrich, Co.) in PBS, pH 7.4, for one hour, washed two times with deionized water, and stained with HQ Silver™ silver enhancement solution (Nanoprobes, Inc) for 15 min followed by a final washing. The tumor sections were finally stained with 3 μM 4′,6-diamidino-2-phenylindole (DAPI) (Molecular Probes, Thermo Fisher Scientific) for two and a half hours to mark cell nuclei. Adjacent tumor slides were fixed in 4% formaldehyde and stained with hematoxylin and eosin (H & E) (Thermo Fisher Scientific and Poly Scientific R & D Corp). The stained section was covered with a drop of mounting medium (Permount®, Fisher Scientific) and then a cover slide was placed over the medium. The slides were examined under an inverted fluorescence microscope (IX71 Olympus).

3. Results

We have synthesized and investigated pHLIP® and PEG coated gold nanoparticles. In our study we used WT pHLIP® peptide (4.1 kDa) with a single Cys residue at the N-terminus and similar size of PEG polymer (about 5 kDa) with a single SH group. The pHLIP® and PEG were used in a mixture with reducing agents, tri-sodium citrate or ascorbic acid, to prepare spherical or spiked gold nanoparticles, respectively. The pHLIP® peptide was dissolved in a solution of 2.7 M urea and mixed (in equal parts) with degassed, deionized water containing a ten times molar-excess of TCEP, which prevents the formation of disulfide bonds. The PEG polymer was dissolved in degassed, deionized water containing a ten times molar-excess of TCEP.

3.1. Synthesis and characterization of spherical pHLIP® and PEG coated gold nanoparticles

To obtain pHLIP® and PEG coated spherical gold nanoparticles, the solution of gold III chloride was reduced using tri-sodium citrate mixed with pHLIP® peptide and PEG polymer. The solution containing gold III chloride, citrate, pHLIP®, and PEG was blown with argon and sealed for incubation at room temperature. Within 15–20 min a change in color of the solution was observed (Supplementary Fig. S1) and particles were left overnight at room temperature to ensure the complete reduction of the gold and coating of nanoparticles by pHLIP® and PEG. Interesting to note that presence of pHLIP® slows down time of gold reduction.

In the course of this study we varied the amount of citrate, pHLIP®, and PEG, and monitored the changes of nanoparticles size and absorbance of the nanoparticles solution for the appearance of a resonance peak at 525 nm (Fig. 1). The absence of pHLIP® and PEG leads to the aggregation of particles and precipitation within a couple of hours after their preparation (Supplementary Fig. S1 and Fig. 1a). The higher amount of citrate is expected to promote better stability of nanoparticles. However our goal was an investigation of formation of gold nanoparticles in the presence of pHLIP® and PEG, which were found to enhance stability and solubility of nanoparticles. The best resonance was observed when gold nanoparticles were coated with both pHLIP® and PEG. The amount of sodium citrate was varied from 0.42% to 2.8% wt/vol in the presence of 10% pHLIP® and 90% PEG in solution, where the concentration of citrate is reported as a final concentration in the nanoparticle solution (Fig. 1b). A low amount of citrate (0.42% wt/vol) in solution results in the shift and broadening of the resonance peak, as well as the appearance of large particles, which was confirmed by the nanoparticle tracking system (data not shown). At the same time, particle sizes did not change when the amount of citrate was varied from 0.83% wt/vol to 2.8% wt/vol. The best results (narrow resonance) were obtained for citrate concentrations in the range between 0.83% wt/vol and 1.7% wt/vol. There is a possibility that at high amount of citrate (2.8% wt/vol) in the presence of pHLIP® and PEG, the shape of particles might be altered, which leads to the broadening and shift of a resonance.

The amount of pHLIP® peptide and PEG polymer was altered as well. An increased percentage of negatively charged pHLIP®, which slows down process of gold reduction, and decreased percentage of neutral PEG polymer leads to the broadening of resonance and shift (by 6–8 nm) of resonance to longer wavelengths (Fig. 1c). The minimum amount of citrate (0.83% wt/vol), 10% pHLIP® and 90% PEG were chosen as an optimal, when resonance is narrow and there are enough of pHLIP® peptides deposited to the surface of nanoparticles to preserve pH-dependent interaction of the coated nanoparticles with the lipid bilayer of a membrane. The final selected composition of reagents (0.83% citrate and 10% pHLIP-90% PEG) comprised the following molar parts: 0.5 parts of 10 mM gold III chloride; 0.075 parts of tri-sodium citrate (10% wt/vol); 0.1125 parts of 0.5 mM PEG with 5 mM TCEP; 0.0125 parts 0.5 mM pHLIP® peptide with 5 mM TCEP and 1.35 M urea, and 0.3 parts of degassed deionized water.

After synthesis, the solution of nanoparticles was purified to remove large particles and excess reducing agents. The large particles were removed by centrifugation. The excess reducing agents were removed when the nanoparticles were transferred to PBS, pH 7.4 solution by size-exclusion chromatography. TEM imaging was employed to analyze

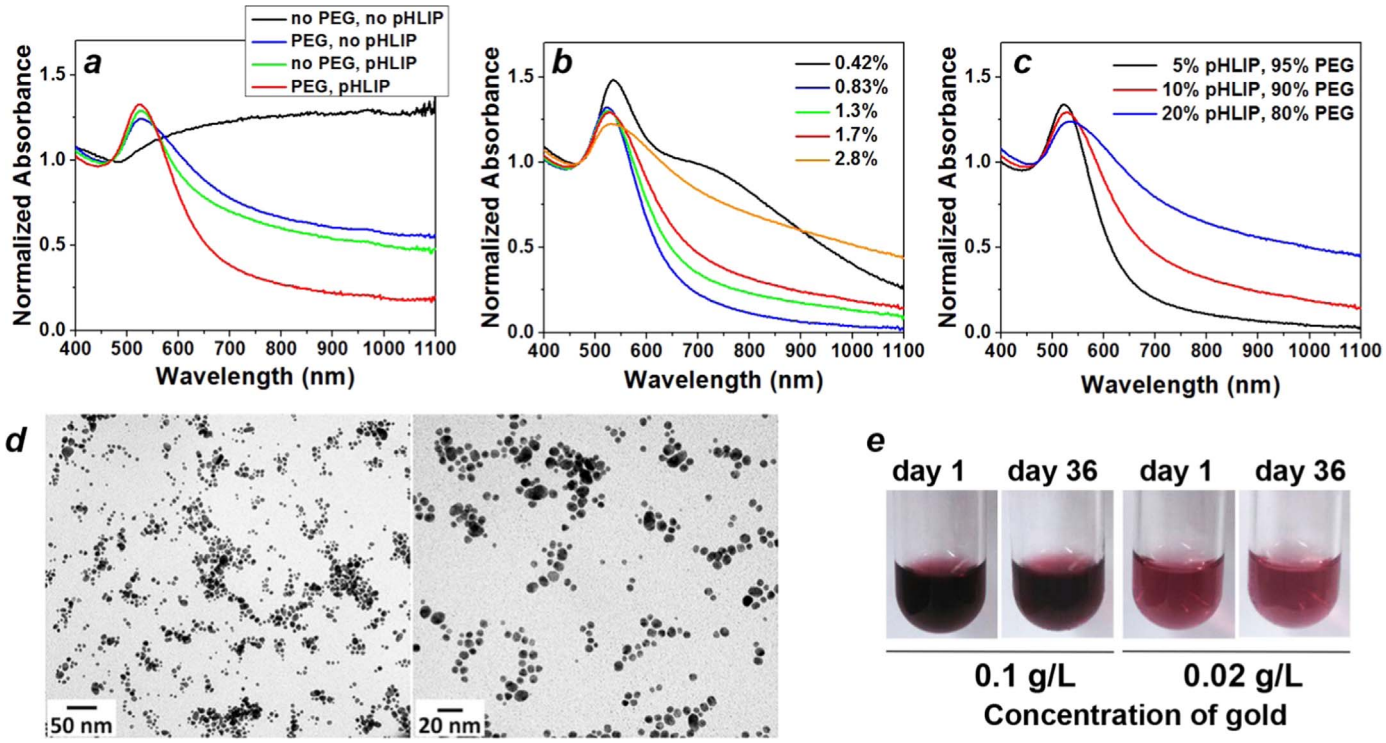

Fig. 1. *Characterization of Spherical Gold Nanoparticles.* The absorbance spectra of the spherical gold nanoparticle solutions synthesized *a*) in the absence and presence of pHLIP® peptide and/or PEG polymer or mixture of 10% pHLIP® and 90% PEG (1.7% wt/vol citrate); *b*) with various amounts of sodium citrate, where the percentage of citrate is reported as the final wt/vol concentration (10% pHLIP® and 90% PEG); *c*) with various amounts of pHLIP® and PEG (0.83% wt/vol citrate). *d*) The representative TEM images of pHLIP® and PEG coated spherical gold nanoparticles obtained at 20,000× and 40,000x magnifications (0.83% wt/vol citrate and 10% pHLIP® – 90% PEG). The size histograms of the metallic core of pHLIP® and PEG coated nanoparticles is shown in Supplementary Fig. S2a. *e*) White light images of particles at the beginning and end of stability studies (0.83% wt/vol citrate and 10% pHLIP® – 90% PEG, particles were purified and kept at 4 °C in PBS, pH 7.4).

nanoparticle size and shape distributions (Fig. 1e). The nanoparticles were homogeneous and round. The metallic core was about 7.0 ± 2.5 nm in diameter (Supplementary Fig. S2a). The mean hydrodynamic size (diameter), determined by nanoparticle tracking system, was about 43 nm.

Purified spherical gold nanoparticles coated with pHLIP® and PEG (0.83% citrate and 10% pHLIP-90% PEG) were stable for at least 36 days at 4 °C in PBS, pH 7.4. The stability of gold nanoparticles in solution was assessed by visual appearance of precipitate, measurements of nanoparticle size and resonance peak by absorbance recording. The stability study was carried out on the particles at two different concentrations with gold amount of 0.10 g/L and 0.02 g/L. A high stability profile was obtained for both concentrations (Fig. 1d). At the same time, when particles were synthesized using a citrate reducing agent (low amount of citrate) containing only PEG, or without both PEG and pHLIP®, the stability was seriously compromised; particles settled over time forming large visible aggregates and the resonance peak was shifted and broadened (data not shown). Thus, the presence of pHLIP® peptide in gold nanoparticles coating is essential to maintain colloidal stability over time when using the methods described here.

3.2. Templated synthesis and characterization of pHLIP® and PEG coated multispiked gold nanoparticles

Another approach we explored in the preparation of pHLIP® and PEG coated gold nanoparticles was based on use of bicelles as a soft template, to obtain irregularly shaped nanoparticles. Bicelles are disk-like micelles, which consist of long-chain and short-chain phospholipids or surfactants (Fig. 2a). The limitation in experiments using bicelles is typically the high critical micelle concentration (CMC) of lipids and detergents, which restricts the degree of bicelle dilution without the lipid phase transforming to vesicles. For example, the CMC of the widely used short-chain D6PC lipid is 14 mM. Thus, when the best characterized system of D6PC–DMPC bicelles are diluted below CMC, they are expected to be converted into a mixture of free D6PC lipids and DMPC lipid bilayer liposomes. It is known that D7PC lipids have a 10 times lower CMC (1.4 mM), and D7PC–DMPC mixtures retain bicelle properties at concentrations even as low as 0.1% wt/vol [39]. Therefore, we selected the DMPC-D7PC lipid system and ensured that the addition of gold and reducing solutions does not lead to the dilution of lipids below 0.1% wt/vol. Assuming the DMPC and DHPC head groups occupy the same areas, the molar ratio of long-chain to short-chain lipids is expressed via *q*-values, which reflects different aspect ratios of disk-like bicelles [40,41]:

$$q = \frac{[DMPC]}{[DHPC]} = \frac{2\pi R^2}{\pi h(\pi R + h)}$$

where R is the radius and h is the height of the bicelle (Fig. 2a). The height of the bicelles in our study was 4.2 nm and the radius varied depending upon the ratio of DMPC to DHPC lipids. The diameters of the bicelles of different asymmetry, $d(q)$, calculated according to the above equation (without accounting for the DHPC capping) are the following: $d(0.2) = 4.2$ nm; $d(0.3) = 6.0$ nm; $d(0.5) = 8.6$ nm; $d(0.75) = 12$ nm; and $d(1.0) = 15$ nm. To investigate the integrity of the D7PC-DMPC bicelle structures of various aspect ratios, we monitored their change in size at concentrations of 1.0%, 0.5% and 0.1% wt/vol (Fig. 2b). Because we were only concerned with the change in size upon dilution, no attempts were made to account for asymmetric particle sizes in DLS measurements. A slight increase in size was observed at low concentrations (0.1% wt/vol) for bicelles with *q*-values less than 0.75. On the other hand, highly asymmetric bicelles with a *q*-value equal to 1 lose their structural integrity as a result of dilution. Therefore, all experiments were performed with bicelles of *q*-values of 0.75 and lower.

Templated synthesis of pHLIP® and PEG coated multispiked gold

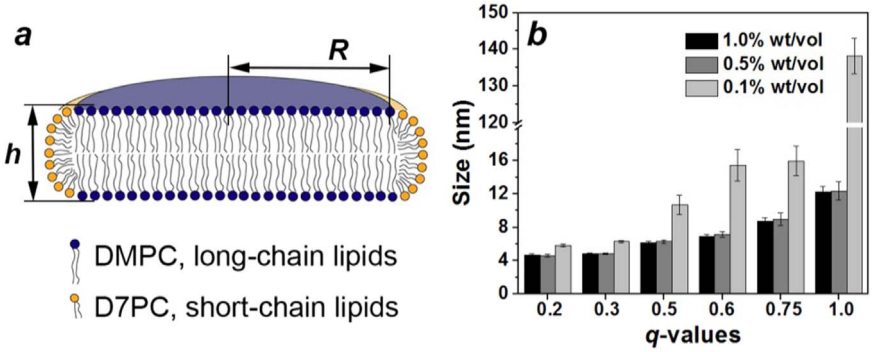

Fig. 2. *Structure of bicelles. a*) The disk-like shape of a bicelle with height, *h*, and radius, *R*, composed of DMPC and DHPC lipids. *b*) Dependence of bicelle size, established by DLS, on its *q*-value, which is a ratio of long- to short-chain lipids (reflecting the asymmetry of a bicelle).

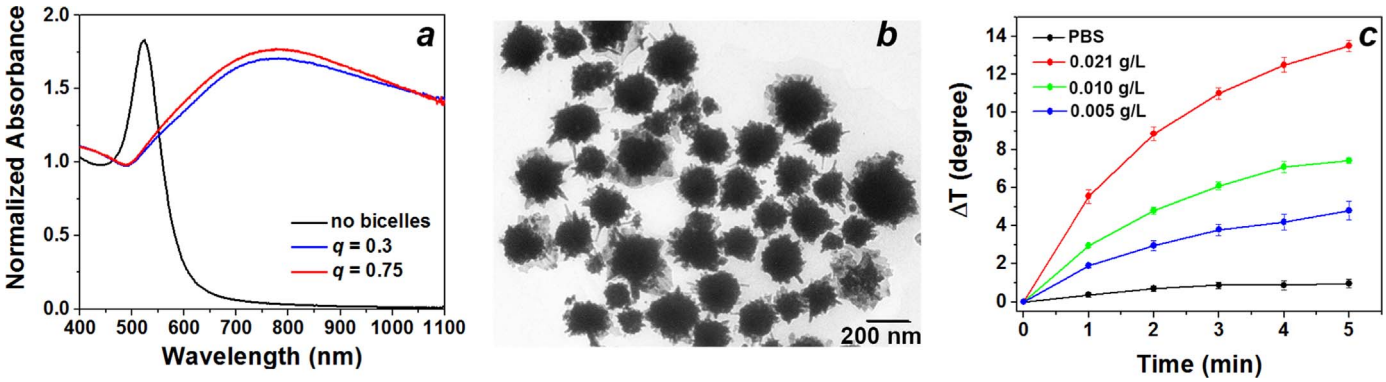

Fig. 3. *Characterization of Multispiked Gold Nanoparticles. a*) The absorbance spectra of gold nanoparticles obtained by gold reduced with ascorbic acid, pHLIP®, and PEG in the absence and presence of bicelles of different asymmetries. *b*) The representative TEM image of pHLIP® and PEG coated multispiked gold nanoparticles obtained at 12,000× magnification. The size histograms of the metallic core of pHLIP® and PEG coated nanoparticles is shown in Supplementary Fig. S2b. *c*) The change in temperature over time measured in solutions containing pHLIP® and PEG coated spiked gold nanoparticles of different concentrations irradiated by an 805 nm laser.

nanoparticles was always initiated shortly after bicelle preparation. We ensured that the addition of gold solution and reducing agents does not lead to the dilution of the bicelle solution to lipid concentrations less than 0.1% wt/vol. The following steps were performed in synthesis of multispiked gold nanoparticles: i) a solution of gold III chloride was added to the solution of bicelles and mixed; ii) next, the reducing agent, ascorbic acid, was added very carefully; and iii) upon color change (~30 s) the solution containing pHLIP® and PEG was immediately added to complete the coating process. The appearance of NIR absorbance (Fig. 3a) along with TEM imaging (Fig. 3b) was indicative of the formation of multispiked gold nanoparticles. In the absence of bicelles, the resonance shifted to 525 nm (Fig. 3a), reflecting the formation of solid spherical gold nanoparticles, which was also confirmed by TEM. Interestingly, the use of citrate as a reducer instead of ascorbic acid shifts the equilibrium towards the formation of solid spherical gold particles rather than the templated synthesis of spiked gold nanoparticles (data not shown). The change of bicelle asymmetry (increase of *q*-values from 0.3 to 0.75) does not affect appearance of NIR resonance (Fig. 3a). Variation in the amount of gold in the range from 1:0.5 to 1:3 lipid:gold ratios did not significantly affect the appearance of the resonance peak. The normalized absorbance of nanoparticles does not change upon dilution or the addition of a detergent that disrupts lipid structures, Triton X-100, indicating nanoparticle stability and integrity after synthesis (data not shown). The presence of pHLIP® and PEG resulted in the formation of particles that were more stable in aqueous solution compared to the particles without coating, which were precipitated shortly after their preparation. The final composition of the reagents was the following molar parts: 0.05 part of 15 mM of lipids arranged into bicelles (> 0.1% wt/vol), 0.15 parts of 5 mM gold III chloride; 0.0225 parts of 250 mM ascorbic acid; 0.414 parts of 0.5 mM PEG with 5 mM TCEP; 0.046 parts 0.5 mM pHLIP® peptide with 5 mM TCEP and 1.35 M urea; and 0.3175 parts of degassed, deionized water.

TEM imaging performed on filtered pHLIP® and PEG coated gold nanoparticles demonstrated the presence of irregular, multispiked gold nanoparticles (Fig. 3b). The structures were the same for bicelles with different *q*-values. Conversely, multispiked structures were not observed in absence of bicelles. The mean core size (diameter) of multispiked nanoparticles established by TEM was 146.0 ± 50.4 nm (Supplementary Fig. S2b). The mean hydrodynamic diameter, determined by nanoparticle tracking system, was about 161 nm.

Different concentrations of pHLIP® and PEG coated multispiked gold nanoparticles were illuminated in solution by an 805 nm laser diode with 500 mW output. The laser radiant exposure was ~400 J/cm^2. For particles at a concentration of 0.021 g/L gold, a temperature increase of 14 degree units (from 26 °C to 40 °C) was observed within 5 min (Fig. 3c), which is ~18 J imparted to water or ~12% energy converted to heat. More concentrated particles showed greater temperature changes at all time points compared to less concentrated particles.

3.3. Interaction of pHLIP® and PEG coated gold nanoparticles with cancer cells

First, we have tested the cytotoxicity of pHLIP® and PEG coated spherical and multispiked gold nanoparticles. JC murine mammary-gland adenocarcinoma cells were treated with gold nanoparticles (0.025 and 0.013 g/L of spherical; and 0.010 g/L and 0.005 g/L of multispiked) for 48 h. The obtained results indicate that these gold nanoparticles do not exhibit any cellular toxicity.

Next, we evaluated the pH-dependent cellular uptake of spherical gold nanoparticles coated with pHLIP® and PEG. The experiment was performed several times and in different ways, such that the treatment

of cells with gold nanoparticles was done at neutral and low pH, or the pre-treatment of cells with gold nanoparticles was done at neutral pH followed by the change of pH with media to low pH. All obtained data indicate that the uptake of spherical gold nanoparticles coated with pHLIP® and PEG by JC cancer cells at pH 6.0 was about 3 times higher than the uptake at neutral pH. The results confirm the pH-dependent cellular uptake of gold nanoparticles coated with pHLIP® and PEG.

3.4. Distribution of pHLIP® and PEG coated gold nanoparticles within tumors

JC cancer cells were inoculated into the right flank of mice by subcutaneous injection. Spherical gold nanoparticles coated with pHLIP® and PEG were administered as a single intra-tumoral injection at quantities of 5.5 and 21 μg gold. One hour after injection, animals were sacrificed so that tumors could be collected and processed to establish the amount of gold within and the distribution throughout a tumor. Among all of the mice, there were animals with different tumor masses that were separated into 3 groups: 0.1, 0.3 and 0.4 g. The percentage of injected dose accumulated within the tumors increased with the increase of tumor mass: 16.2% for 0.1 g tumor; 18.0% for 0.3 g, and 29.1% for 0.4 g of tumor (Supplementary Fig. S3). The mean tumor uptake of gold (calculated for 8 animals) was 6.8 μg of gold per gram of tumor (with standard error of 1.6) when a total of 5.5 μg of gold was injected. The mean tumor uptake of gold (calculated for 6 animals) was 24.5 μg/g (with standard error of 8.5) when 21 μg of gold was injected. The highest accumulation of gold ~47 μg/g was found in the smallest tumors (85.0 ± 2.3 mg) injected with 21 μg of gold.

We also investigated the distribution of gold within the tumor mass. The white light images were taken from the center of the tumor mass (Fig. 4a). Then, the frozen tumor samples were sectioned and stained with H & E (Fig. 4b). The gold was distributed nearly homogeneously within tumor mass except the right edge of the tumor with no gold accumulation in the surrounding muscle. The muscle tissue adjacent to the tumor is indicated by arrows on Fig. 4a and b, and a magnified image of the border of the section containing both cancer cells and muscle is shown on Fig. 4c. Adjacent sections were treated with Triton to permeabilize the cellular membranes and then stained with both a silver enhancement solution and DAPI. The representative images of the gold enhanced by silver and stained nuclei are shown on Fig. 4d–f.

4. Discussion

The motivation for our work was based on a desire to introduce stable pH-sensitive pHLIP® and PEG coated gold nanoparticles with a potential translation to the clinic. We developed methods for the preparation of spherical and multispiked gold nanoparticles coated with pHLIP® and PEG, which might find application in radiation and NIR thermal therapies. The approach for the synthesis of spherical gold nanoparticles coated with pHLIP® and PEG is very robust and can be implemented in applied studies. The protocol for the preparation of multispiked gold nanoparticles coated with pHLIP® and PEG could be further optimized, however the proof of principle is established in our work. In both cases, pHLIP® peptide and PEG polymer were used as components of the reducing solution (sodium citrate as a reducer in the case of spherical nanoparticles and ascorbic acid in the case of multi-spiked nanoparticles). The optimal combination of pHLIP® and PEG was selected to be 10% and 90%, respectively. A decreased percentage of pHLIP® in the nanoparticle coating might lead to the reduction of particle stability (resulting from the reduction of the overall negative charge due to the presence of pHLIP® peptide on particle surfaces) and the loss of pH-dependent properties. Previously, we investigated and showed the utility of liposomes coated with different quantities of pHLIP® and PEG [30,35]. It is also possible to further optimize particles

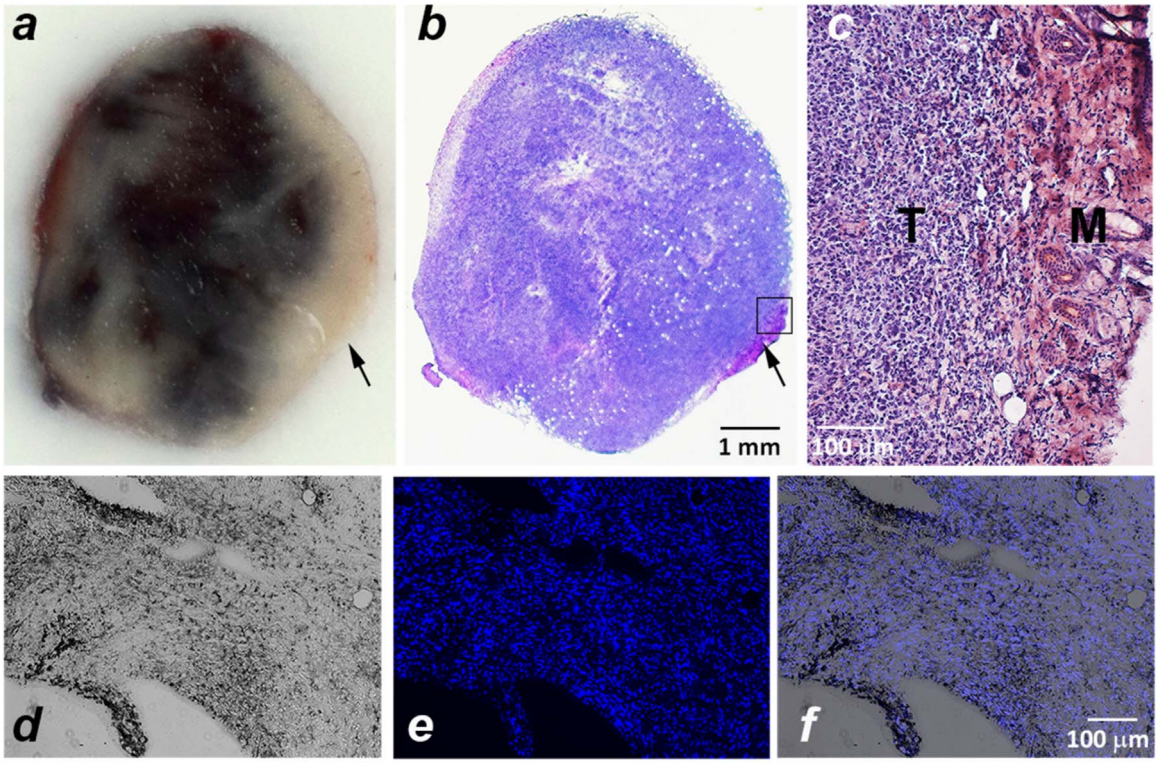

Fig. 4. *Tumor Imaging of Spherical Gold Nanoparticle Uptake. a*) The white light image of a tumor center showing the gold distribution (after a 21 μg intra-tumoral injection of pHLIP® and PEG coated spherical gold nanoparticles in PBS, pH7.4); *b*) the section from the tumor center stained with H & E; and *c*) the magnified image of the tumor section outlined by a square in panel *b*, which shows tumor (T) and muscle (M). The arrows on panels *a* and *b* indicate muscle tissue. *d*) The bright field image of tumor sections stained with silver enhancement solution and *e*) the fluorescent image of the same tumor section stained with DAPI to visualize cell nuclei; and *f*) an overlay of the bright filed and fluorescent images. The percentage of injected dose of gold accumulated within tumors of different masses is given in the text and in Supplementary Fig. S3.

by employing a pHLIP® PEG conjugate instead of directly coating the surface with pHLIP®. Spherical gold nanoparticles coated with pHLIP® and PEG exhibited high stability in solution over a one month time period, as opposed to the particles with no coating or just PEG coating. The PEG coating was widely utilized in coating of various nanoparticles [42–46]. The size of the pHLIP® PEG coated particles' metallic core was in the range of 5–8 nm in diameter and the hydrodynamic size (diameter) of coated particles was in the range of 40–50 nm. The nanoparticles showed a pH-dependent uptake by cancer cells with no signs of cytotoxicity. We performed intra-tumoral injections of spherical gold nanoparticle solutions and investigated gold uptake and distribution within tumors at one hour post-injection. It does not seem that there is any clinical utility to perform a systemic administration of particles, since radiation therapy is typically delivered locally and the location of the tumor is known from prior diagnostic imaging. Also, there is a requirement to have as much gold as possible within a tumor (which could be achieved only by local administration of the particles) to induce a radiation enhancement effect. The radiation delivered within a one hour time frame of particle administration is expected to be in line with clinical practice. Our results indicate that gold nanoparticles (21 μg of injected gold) were distributed within the tumor mass very well and with an overall uptake of 24.5 μg of gold per gram of tumor mass, reaching values of 47 μg/g in tumors with masses of 1 g and less. This is a higher uptake compared to that of pHLIP® gold nanoclusters [37]. We believe, the presence of pHLIP® peptide in the coating of gold nanoparticles was crucial. The peptide allowed particles to stay within the tumor and promoted the uptake of particles by cancer cells at low extracellular pH, as we have shown previously [37,38]. At the same time, particles were able to diffuse within a tumor as opposed to the direct injection of micron-sized gold particles, that hinder tumor coverage by staying only at the injection site [3]. We also would like to outline that systemic administration of nanoparticles or antibodies conjugated with gold nanoparticles results in staining of only the peripheral tumor regions with limited penetration inside the tumor mass [47]. We did not observe an accumulation of gold within the muscle tissue adjacent to the tumors. The amount of injected gold in our study was much less than the amount of gold used in previous radiation therapy studies on mice (see review and references within it) [48]. However, we believe that the targeting of gold nanoparticles directed by pHLIP® peptide to the vital cellular structures such as plasma and nuclear membranes could lead to the enhancement of radiation effects even at lower gold concentrations [38].

The spherical particles have the smallest surface to volume ratio for a given size of a particle. The appearance of multiple sharp spikes or tips on the surface of nanoparticle is known to give rise to the strong spatial confinement of the electromagnetic field, since the core of a particle serves as a nanoscale antenna, increasing the excitation cross section and the enhancement of the tip plasmon polaritons [49,50]. Various approaches were introduced in the synthesis of star-like and multispiked gold nanoparticles [50–53]. We used a soft template material of phospholipid bicelles to synthesize pHLIP® and PEG coated multispiked gold nanoparticles. Bicelles, which possess both low- and high- curvature regions within a bilayer disks, represent a class of model membranes used in nuclear magnetic resonance (NMR) structural studies of membrane biomolecules [41,54–56], but they have found additional applications in biomedical sciences [57–59]. The bicellar templates were utilized previously to control the growth of platinum with ascorbic acid as a reducer, producing metal nanodisks and nanowheels [60,61]. Other phospholipid structures, like spherical liposomes, were also used for gold deposition to assemble biodegradable plasmon resonant nanoshells, which were used for the laser-induced release of molecules encapsulated into these liposomes [62–64]. Another approach was based on the assembly of liposomes and micelles, called metallosomes, by using lipids conjugated with gold nanoclusters [65]. The presence of a soft template, like bicelles, in our reduction mixture induced the formation of multispiked gold nanoparticles with plasmon resonance in the NIR range. The absence of bicelles leads to the formation of spherical gold nanoparticles with absorbance at 525–560 nm. The size of gold multispiked nanoparticles established by TEM imaging and nanoparticle tracking system was in the range of 100–170 nm and 130–200 nm, respectively. The heating of pHLIP® and PEG coated multispiked gold nanoparticles in solution by an 805 nm laser diode led to the increase of the solution temperature by 14 degrees within 5 min. Multispiked particles could be used in combination with NIR laser treatment for photo-induced hyperthermia. It would be very advantageous to employ lower power NIR laser radiation systems, which are currently available for indocyanine green (ICG) imaging in clinical endoscopy and laparoscopy (see table 4 for the description of IC G clinical imaging systems in the review article) [66]. Also, due to the very high surface area of multispiked gold nanoparticles, we envision their potential successful application for the enhancement of x-ray radiation effects. A number of binary radiation therapies are under consideration [2,67–69]. At low photon energies, the most promising approach is based on dose enhancement through Auger electron emission. Auger electron emission generates a cascade of low energy electrons that travel short distances and deposit their energy locally [70]. Thus, it is very important to deliver gold nanoparticles to vital cellular structures, which pHLIP® helps achieve. Also, it was proposed that a potential advantage of the use of small gold nanoparticles (with an enhanced surface/volume ratio) is the minimization of the energy of the Auger electrons deposited (lost) inside the gold nanoparticle [38,70]. Therefore, it could be very attractive to test multispiked gold nanoparticles with large surface/volume ratios as radiation enhancers.

Author contributions

JL Daniels, OA Andreev, and YK Reshetnyak designed the research; JL Daniels and TM Crawford performed the research; JL Daniels, TM Crawford, and YK Reshetnyak analyzed the data; JL Daniels and YK Reshetnyak wrote the paper.

Conflict of interest

OA Andreev and YK Reshetnyak have founded and have a financial interest in a company, pHLIP, Inc., with the aim of bringing pHLIP® technology to the clinic. The company has had no involvement in funding the studies reported here.

Acknowledgment

We are grateful to Renato Guerrieri for his assistance in preliminary experiments in the preparation of multispiked gold nanoparticles. We would like to thank Dr. Al Bach and Kim Andrews, Rhode Island IDeA Network for Excellence in Biomedical Research (INBRE), as well as Dr. Katherine Kelley, University of Rhode Island, the Graduate School of Oceanography, for their assistance in ICP-MS analysis of samples; Dr. Richard Kingsley and Dr. Iftheker Khan, University of Rhode Island, for performing TEM imaging; Dr. Anna Moshnikova, University of Rhode Island, for her assistance with studies on cultured cells; and Dr. Michael Anderson, University of Massachusetts Boston, for his discussions concerning heating experiments. This work was supported by the General Medical Sciences of the National Institutes of Health grant R01GM073857 to OAA and YKR. Also, this research was supported in part by an Institutional Development Award (IDeA) Network for Biomedical Research Excellence from the National Institute of General Medical Sciences of the National Institutes of Health under grant number P20GM103430.

Appendix A. Transparency document

Transparency document associated with this article can be found in the online version at doi:10.1016/j.bbrep.2017.02.008.

References

[1] J.F. Hainfeld, F.A. Dilmanian, D.N. Slatkin, H.M. Smilowitz, Radiotherapy enhancement with gold nanoparticles, J. Pharm. Pharm. 60 (8) (2008) 977–985.
[2] J.F. Hainfeld, D.N. Slatkin, H.M. Smilowitz, The use of gold nanoparticles to enhance radiotherapy in mice, Phys. Med. Biol. 49 (18) (2004) N309–315.
[3] D.M. Herold, I.J. Das, C.C. Stobbe, R.V. Iyer, J.D. Chapman, Gold microspheres: a selective technique for producing biologically effective dose enhancement, Int. J. Radiat. Biol. 76 (10) (2000) 1357–1364.
[4] P. Retif, S. Pinel, M. Toussaint, et al., Nanoparticles for radiation therapy enhancement: the key parameters, Theranostics 5 (9) (2015) 1030–1044.
[5] D.P. O'Neal, L.R. Hirsch, N.J. Halas, J.D. Payne, J.L. West, Photo-thermal tumor ablation in mice using near infrared-absorbing nanoparticles, Cancer Lett. 209 (2) (2004) 171–176.
[6] G. von Maltzahn, J.H. Park, A. Agrawal, et al., Computationally guided photothermal tumor therapy using long-circulating gold nanorod antennas, Cancer Res. 69 (9) (2009) 3892–3900.
[7] E.B. Dickerson, E.C. Dreaden, X. Huang, et al., Gold nanorod assisted near-infrared plasmonic photothermal therapy (PPTT) of squamous cell carcinoma in mice, Cancer Lett. 269 (1) (2008) 57–66.
[8] C. Xu, S. Sun, Superparamagnetic nanoparticles as targeted probes for diagnostic and therapeutic applications, Dalton Trans. 29 (2009) 5583–5591.
[9] R.A. Bohara, N.D. Thorat, S.H. Pawar, Role of functionalization: strategies to explore potential nano-bio applications of magnetic nanoparticles, RSC Adv. 6 (2016) 43989–44012.
[10] N.D. Thorat, R.A. Bohara, S.A. Tofail, et al., Superparamagnetic gadolinium ferrite nanoparticles with controllable curie temperature – cancer theranostics for mr-imaging-guided magneto-chemotherapy, Eur. J. Inorg. Chem. (2016) 4586–4597.
[11] R.A. Bohara, N.D. Thorat, H.M. Yadav, S.H. Pawar, One-step synthesis of uniform and biocompatible amine functionalized cobalt ferrite nanoparticles: a potential carrier for biomedical applications, New J. Chem. 38 (2014) 2979–2986.
[12] D. Ho, X. Sun, S. Sun, Monodisperse magnetic nanoparticles for theranostic applications, Acc. Chem. Res. 44 (10) (2011) 875–882.
[13] L.M. Lacroix, D. Ho, S. Sun, Magnetic nanoparticles as both imaging probes and therapeutic agents, Curr. Top. Med Chem. 10 (12) (2010) 1184–1197.
[14] P.R. Srinivas, B.S. Kramer, S. Srivastava, Trends in biomarker research for cancer detection, Lancet Oncol. 2 (11) (2001) 698–704.
[15] J.P. Janssens, I. Verlinden, N. Gungor, J. Raus, L. Michiels, Protein biomarkers for breast cancer prevention, Eur. J. Cancer Prev. 13 (4) (2004) 307–317.
[16] J.H. Hanke, K.R. Webster, L.V. Ronco, Protein biomarkers and drug design for cancer treatments, Eur. J. Cancer Prev. 13 (4) (2004) 297–305.
[17] S.J. Goldsmith, Receptor imaging: competitive or complementary to antibody imaging? Semin Nucl. Med. 27 (2) (1997) 85–93.
[18] B. Freimark, D. Clark, F. Pernasetti, et al., Targeting of humanized antibody D93 to sites of angiogenesis and tumor growth by binding to multiple epitopes on denatured collagens, Mol. Immunol. 44 (15) (2007) 3741–3750.
[19] L.E. Gerweck, K. Seetharaman, Cellular pH gradient in tumor versus normal tissue: potential exploitation for the treatment of cancer, Cancer Res. 56 (6) (1996) 1194–1198.
[20] N. Raghunand, M.I. Altbach, R. van Sluis, et al., Plasmalemmal pH-gradients in drug-sensitive and drug-resistant MCF-7 human breast carcinoma xenografts measured by 31P magnetic resonance spectroscopy, Biochem. Pharmacol. 57 (3) (1999) 309–312.
[21] D. Weerakkody, A. Moshnikova, M.S. Thakur, et al., Family of pH (low) insertion peptides for tumor targeting, Proc. Natl. Acad. Sci. USA 110 (15) (2013) 5834–5839.
[22] O.A. Andreev, D.M. Engelman, Y.K. Reshetnyak, Targeting diseased tissues by pHLIP insertion at low cell surface pH, Front. Physiol. 5 (2014) 97.
[23] Y.K. Reshetnyak, O.A. Andreev, U. Lehnert, D.M. Engelman, Translocation of molecules into cells by pH-dependent insertion of a transmembrane helix, Proc. Natl. Acad. Sci. USA 103 (17) (2006) 6460–6465.
[24] Y.K. Reshetnyak, M. Segala, O.A. Andreev, D.M. Engelman, A monomeric membrane peptide that lives in three worlds: in solution, attached to, and inserted across lipid bilayers, Biophys. J. 93 (7) (2007) 2363–2372.
[25] O.A. Andreev, A.D. Dupuy, M. Segala, et al., Mechanism and uses of a membrane peptide that targets tumors and other acidic tissues in vivo, Proc. Natl. Acad. Sci. USA 104 (19) (2007) 7893–7898.
[26] A.G. Karabadzhak, D. Weerakkody, D. Wijesinghe, et al., Modulation of the pHLIP transmembrane helix insertion pathway, Biophys. J. 102 (8) (2012) 1846–1855.
[27] R.C. Adochite, A. Moshnikova, S.D. Carlin, et al., Targeting breast tumors with pH (low) insertion peptides, Mol. Pharm. 11 (8) (2014) 2896–2905.
[28] Z. Cruz-Monserrate, C.L. Roland, D. Deng, et al., Targeting pancreatic ductal adenocarcinoma acidic microenvironment, Sci. Rep. 4 (2014) 4410.
[29] A.G. Karabadzhak, M. An, L. Yao, et al., pHLIP-FIRE, a cell insertion-triggered fluorescent probe for imaging tumors demonstrates targeted cargo delivery in vivo, ACS Chem. Biol. 9 (11) (2014) 2545–2553.
[30] L. Yao, J. Daniels, D. Wijesinghe, O.A. Andreev, Y.K. Reshetnyak, pHLIP(R)-mediated delivery of PEGylated liposomes to cancer cells, J. Control Release 167 (3) (2013) 228–237.
[31] F. Emmetiere, C. Irwin, N.T. Viola-Villegas, et al., (18)F-labeled-bioorthogonal liposomes for in vivo targeting, Bioconjug. Chem. 24 (11) (2013) 1784–1789.
[32] L. Han, H. Ma, Y. Guo, Y. Kuang, X. He, C. Jiang, pH-controlled delivery of nanoparticles into tumor cells, Adv. Health. Mater. (2013).
[33] M. Yu, F. Guo, J. Wang, F. Tan, N. Li, A pH-Driven and photoresponsive nanocarrier: remotely-controlled by near-infrared light for stepwise antitumor treatment, Biomaterials 79 (2016) 25–35.
[34] M. Yu, F. Guo, J. Wang, F. Tan, N. Li, Photosensitizer-loaded pH-responsive hollow gold nanospheres for single light-induced photothermal/photodynamic therapy, A CS Appl Mater. Interfaces 7 (32) (2015) 17592–17597.
[35] D. Wijesinghe, M.C. Arachchige, A. Lu, Y.K. Reshetnyak, O.A. Andreev, pH dependent transfer of nano-pores into membrane of cancer cells to induce apoptosis, Sci. Rep. 3 (2013) 3560.
[36] B. Janic, M.P. Bhuiyan, J.R. Ewing, M.M. Ali, pH-dependent cellular internalization of paramagnetic nanoparticle, ACS Sens. 1 (8) (2016) 975–978.
[37] L. Yao, J. Daniels, A. Moshnikova, et al., pHLIP peptide targets nanogold particles to tumors, Proc. Natl. Acad. Sci. USA 110 (2) (2013) 465–470.
[38] M.P. Antosh, D.D. Wijesinghe, S. Shrestha, et al., Enhancement of radiation effect on cancer cells by gold-pHLIP, Proc. Natl. Acad. Sci. USA 112 (17) (2015) 5372–5376.
[39] Z. Lu, W.D. Van Horn, J. Chen, S. Mathew, R. Zent, C.R. Sanders, Bicelles at low concentrations, Mol. Pharm. 9 (4) (2012) 752–761.
[40] P.A. Luchette, T.N. Vetman, R.S. Prosser, et al., Morphology of fast-tumbling bicelles: a small angle neutron scattering and NMR study, Biochim Biophys. Acta 1513 (2) (2001) 83–94.
[41] R.S. Prosser, J.S. Hwang, R.R. Vold, Magnetically aligned phospholipid bilayers with positive ordering: a new model membrane system, Biophys. J. 74 (5) (1998) 2405–2418.
[42] N.D. Thorat, O.M. Lemine, R.A. Bohara, K. Omri, L. El Mir, S.A. Tofail, Superparamagnetic iron oxide nanocargoes for combined cancer thermotherapy and MRI applications, Phys. Chem. Chem. Phys. 18 (31) (2016) 21331–21339.
[43] N.D. Thorat, R.A. Bohara, V. Malgras, et al., Multimodal superparamagnetic nanoparticles with unusually enhanced specific absorption rate for synergetic cancer therapeutics and magnetic resonance imaging, ACS Appl. Mater. Interfaces 8 (23) (2016) 14656–14664.
[44] J.V. Jokerst, T. Lobovkina, R.N. Zare, S.S. Gambhir, Nanoparticle PEGylation for imaging and therapy, Nanomed. (Lond.) 6 (4) (2011) 715–728.
[45] K. Leung, Poly(ethylene glycol)-coated gold nanocages. Molecular Imaging and Contrast Agent Database (MICAD). Bethesda (MD), 2004.
[46] L. Shan, Polyethylene glycol-coated (PEG5000) gold nanoparticles. Molecular Imaging and Contrast Agent Database (MICAD). Bethesda (MD), 2004.
[47] J.F. Hainfeld, M.J. O'Connor, F.A. Dilmanian, D.N. Slatkin, D.J. Adams, H.M. Smilowitz, Micro-CT enables microlocalisation and quantification of Her2-targeted gold nanoparticles within tumour regions, Br. J. Radiol. 84 (1002) (2011) 526–533.
[48] S. Shrestha, L.N. Cooper, O.A. Andreev, Y.K. Reshetnyak, M.P. Antosh, Gold nanoparticles for radiation enhancement in vivo, J. J. Rad. Oncol. 3 (1) (2016) 026.
[49] F. Hao, C.L. Nehl, J.H. Hafner, P. Nordlander, Plasmon resonances of a gold nanostar, Nano Lett. 7 (3) (2007) 729–732.
[50] D. Melnikau, D. Savateeva, A. Susha, A.L. Rogach, Y.P. Rakovich, Strong plasmon-exciton coupling in a hybrid system of gold nanostars and J-aggregates, Nanoscale Res Lett. 8 (1) (2013) 134.
[51] C.L. Nehl, H. Liao, J.H. Hafner, Optical properties of star-shaped gold nanoparticles, Nano Lett. 6 (4) (2006) 683–688.
[52] T.K. Sau, A.L. Rogach, M. Doblinger, J. Feldmann, One-step high-yield aqueous synthesis of size-tunable multispiked gold nanoparticles, Small 7 (15) (2011) 2188–2194.
[53] L. Shao, A.S. Susha, L.S. Cheung, T.K. Sau, A.L. Rogach, J. Wang, Plasmonic properties of single multispiked gold nanostars: correlating modeling with experiments, Langmuir 28 (24) (2012) 8979–8984.
[54] A.A. De Angelis, S.J. Opella, Bicelle samples for solid-state NMR of membrane proteins, Nat. Protoc. 2 (10) (2007) 2332–2338.
[55] T. Raschle, S. Hiller, M. Etzkorn, G. Wagner, Nonmicellar systems for solution NMR spectroscopy of membrane proteins, Curr. Opin. Struct. Biol. 20 (4) (2010) 471–479.
[56] C.R. Sanders, R.S. Prosser, Bicelles: a model membrane system for all seasons? Structure 6 (10) (1998) 1227–1234.
[57] G. Rodriguez, G. Soria, E. Coll, et al., Bicosomes: bicelles in dilute systems, Biophys. J. 99 (2) (2010) 480–488.
[58] L. Barbosa-Barros, G. Rodriguez, C. Barba, et al., Bicelles: lipid nanostructured platforms with potential dermal applications, Small 8 (6) (2012) 807–818.
[59] L. Barbosa-Barros, A. de la Maza, J. Estelrich, et al., Penetration and growth of DPPC/DHPC bicelles inside the stratum corneum of the skin, Langmuir 24 (11) (2008) 5700–5706.
[60] Y. Song, R.M. Dorin, R.M. Garcia, et al., Synthesis of platinum nanowheels using a bicellar template, J. Am. Chem. Soc. 130 (38) (2008) 12602–12603.
[61] R.M. Garcia, Y. Song, R.M. Dorin, et al., Templated growth of platinum nanowheels using the inhomogeneous reaction environment of bicelles, Phys. Chem. Chem. Phys. 13 (11) (2011) 4846–4852.
[62] T.S. Troutman, J.K. Barton, M. Romanowski, Biodegradable plasmon resonant nanoshells, Adv. Mater. 20 (13) (2008) 2604–2608.
[63] S.J. Leung, M. Romanowski, NIR-activated content release from plasmon resonant liposomes for probing single-cell responses, ACS Nano 6 (11) (2012) 9383–9391.
[64] S.J. Leung, M. Romanowski, Light-activated content release from liposomes, Theranostics 2 (10) (2012) 1020–1036.
[65] J.F. Hainfeld, F.R. Furuya, R.D. Powell, Metallosomes, J. Struct. Biol. 127 (2) (1999) 152–160.
[66] J.T. Alander, I. Kaartinen, A. Laakso, et al., A review of indocyanine green fluorescent imaging in surgery, Int. J. Biomed. Imaging 2012 (2012) 940585.
[67] K.N. Morris, M.D. Weil, R. Malzbender, Radiochromic film dosimetry of contrast-enhanced radiotherapy (CERT), Phys. Med. Biol. 51 (22) (2006) 5915–5925.
[68] A. Norman, M. Ingram, R.G. Skillen, D.B. Freshwater, K.S. Iwamoto, T. Solberg, X-ray phototherapy for canine brain masses, Radiat. Oncol. Invest. 5 (1) (1997) 8–14.
[69] G. Tisljar-Lentulis, L.E. Feinendegen, V.P. Bond, Biological radiation effects of inclusion of moderately heavy nuclei into the tissue and use of soft roentgen rays, Strahlentherapie 145 (6) (1973) 656–662.
[70] S.J. McMahon, W.B. Hyland, M.F. Muir, et al., Biological consequences of nanoscale energy deposition near irradiated heavy atom nanoparticles, Sci. Rep. 1 (2011) 18.